Published in final edited form as:
Biomaterials. 2011 December ; 32(34): 8979–8989. doi:10.1016/j.biomaterials.2011.08.037.

The Influence of Elasticity and Surface Roughness on Myogenic and Osteogenic-Differentiation of Cells on Silk-Elastin Biomaterials

Xiao Hu[a,1], **Sang-Hyug Park**[a,1], **Eun Seok Gil**[a], **Xiao-Xia Xia**[a], **Anthony S. Weiss**[b], and **David L. Kaplan**[a,*]

[a]Department of Biomedical Engineering, Tufts University, 4 Colby St. Medford, 02155 MA, USA

[b]School of Molecular Bioscience, The University of Sydney, NSW 20006, Australia

Abstract

The interactions of C2C12 myoblasts and human bone marrow stem cells (hMSCs) with silk-tropoelastin biomaterials, and the capacity of each to promote attachment, proliferation, and either myogenic- or osteogenic-differentiation were investigated. Temperature-controlled water vapor annealing was used to control beta-sheet crystal formation to generate insoluble silk-tropoelastin biomaterial matrices at defined ratios of the two proteins. These ratios controlled surface roughness and micro/nano-scale topological patterns, and elastic modulus, stiffness, yield stress, and tensile strength. A combination of low surface roughness and high stiffness in the silk-tropoelastin materials promoted proliferation and myogenic-differentiation of C2C12 cells. In contrast, high surface roughness with micro/nano-scale surface patterns was favored by hMSCs. Increasing the content of human tropoelastin in the silk-tropoelastin materials enhanced the proliferation and osteogenic-differentiation of hMSCs. We conclude that the silk-tropoelastin composition facilitates fine tuning of the growth and differentiation of these cells.

Introduction

Proteins can be adapted to form a range of diverse biomaterials that have the capacity to control cell differentiation. Human tropoelastin, the precursor of elastin, is present in elastic tissues where it self-assembles and dominates the content of cross-linked elastin networks [1-5]. Elastic tissues differ in their elastin composition as a reflection of functionality. Tropoelastin additionally contains sequences that direct cell-mediated interactions through integrin receptors, and dynamic protein functions driven by environmental factors to modulate mechanical properties [3-6]. At best, these multifunctional features are only partially captured by synthetic elastomers [7]. Through genetic engineering of the gene encoding full-length (60 kDa) human tropoelastin, a unique source of this pure native protein is available in significant quantities [1, 2]. Elastin-based biomaterials are generally considered for short term implants due to proteolytic turnover while many of the design principles are still to be defined in order to achieve mechanical rigidity for longer term

*Corresponding author: David L. Kaplan, david.kaplan@tufts.edu.
[1]Xiao Hu and Sang-Hyug Park contributed equally to this work.

The authors declare no conflict of interest.

physical support during tissue regeneration, such as tendons and ligaments, blood vessels and many other load bearing tissues [1-5].

Most synthetic elastomers are not biologically compatible (e.g., latex, polydimethylsiloxane (PDMS)), lack degradability or biodegradability [7, 8], or lack the biological signaling of native proteins, or are limited by a combination of these limitations. Silk fibroin, a native protein from silkworm fiber, is a remarkably stable and mechanically robust protein biomaterial, as evidenced by the ability to be autoclaved for sterilization; and is amendable to ethylene oxide sterilization and gamma irradiation [9-33]. Silk fibroin can also be cast in versatile formats such as films [19-21], fibers [26], gels [18, 28], sponges [17, 24], particles [25, 27]. These features have paved the way for the adapted use of these protein biomaterials in tissue engineering systems, drug release systems, bio-optics and bioelectronics applications [9-15]. However, silks are limited in terms of elastomeric biomaterial applications due to their inherent tendency to form stiffer materials due to beta sheet crystal formation [9, 16, 29].

The combination of silks and elastins offers an attractive, tailorable family of protein composite systems for a broader range of biomaterial needs such as dynamic matrices for vascular and lung repair, and stronger yet elastic materials for ligaments and tendons [12-15]. As a demonstration of this potential, optimizing the molecular interface between tropoelastin and silk allowed for the generation of novel composite materials [34]. Importantly, the stabilization of these silk-tropoelastin extracellular matrix (ECM) mimics does not require chemical crosslinking due to the strong physical associations that form via beta sheets crystals from the silk chains, as well as specific complexation in the tropoelastin-silk chain interactions [34]. We have also developed options to control the kinetics and extent of the physical crosslinking as part of the induction of beta sheet formation, so further processing options are available such as chemical methods – water vapor annealing, MeOH exposure, low pH; physical methods – sonication, vortexing, electric fields, shear, autoclaving [35]. These changes in physical crosslinks result in controllable mechanical properties and degradation profiles [30, 31, 34, 35].

In the present study, we address the cellular proliferation and osteogenic- and myogenic-differentiation on silk-tropoelastin biomaterials. The focus is on exploiting mechanical stiffness and surface morphology, with the aim of correlating the responses of C2C12 mouse myoblasts and human bone marrow stem cells (hMSCs). This type of insight into biomaterial-cell behavior can provide fine tuning of compositions to optimize specific functional tissue outcomes.

Materials and Methods

Preparation of insoluble silk-tropoelastin films

The preparation of silk fibroin and tropoelastin solutions have been reported previously [34]. *Bombyx mori* silkworm cocoons were boiled in a 0.02 M Na_2CO_3 solution to extract the glue-like sericin proteins [16]. The remaining silk fibroin was dissolved in a 9.3 M LiBr solution at 60°C for 4-6 h, and then dialyzed against distilled water in dialysis cassettes for 2 days. Finally, a 6 wt-% silk fibroin aqueous solution was obtained after centrifugation and filtration. Sequencing grade trypsin, chymotrypsin from bovine pancreas, human neutrophil elastase, and endoproteinase Lys-C were purchased from Calbiochem (EMD Biosciences Inc., San Diego, CA). Recombinant human tropoelastin isoform SHELd26A (Synthetic Human Elastin without domain 26A) was prepared and purified from bacteria on a multi-gram scale, as described previously [1-3]. The amino acid sequence of the 60kDa full-length human tropoelastin protein corresponds to amino acid residues 27–724 of GenBank entry AAC98394 (gi 182020).

Tropoelastin (1.0 wt%) was dissolved in distilled water at 4°C and slowly mixed with diluted 1 wt% silk aqueous solution to avoid protein aggregation. Each of the final 1 wt% blended solutions were based on a mass ratio of silk:tropoelastin = 100:0 (SE100, pure silk) 90:10 (SE90), 75:25 (SE75), 50:50 (SE50), 25:75 (SE25), 10:90 (SE10), and 0:100 (SE0, pure tropoelastin) [34] and were immediately cast on PDMS substrates to form 20~30 μm thick films and kept at 4°C to avoid structural changes in the samples.

Temperature controlled water vapor annealing was used to physically crosslink the silk-tropoelastin films using a heatable vacuum desiccator with temperature controller (Precision Scientific Inc, Chicago, IL) [35]. An aluminum sample basket was fixed in the middle of the desiccator, with the pumping ports connected to a vacuum pump. The bottom of the desiccator was filled with distilled water to generate water vapor in the desiccator during evaporation with relative humidity (RH) above 90%, while the boiling water did not touch the bottom of the sample basket. The temperature controller was first set at a desired annealing temperature (T_c) for several hours until homogenous water vapor was obtained, then the silk-tropoelastin samples were transferred into the desiccator, and the vacuum pump was switched on for 5~10 min after which the vacuum port was turned off to let the homogeneous water vapor anneal the blend samples in the vacuum for 12 hr. Samples were placed in a dry room temperature vacuum oven for two days to remove surface moisture.

Fourier transform infrared spectroscopy (FTIR) analysis

A Jasco (Japan) FT/IR-6200 Spectrometer was equipped with a deuterated triglycine sulfate detector and a multiple reflection, horizontal MIRacle ATR attachment (Ge crystal, Pike Tech). Each measurement incorporated 128 scans (wavenumber from 600 to 4000 cm^{-1}) that were Fourier transformed using a Genzel-Happ apodization function to yield spectra with a nominal resolution of 4 cm^{-1}. Secondary structure peak assignments were as described: absorption bands in the frequency range of 1610~1635 cm^{-1} represent β-sheet structure; absorption bands around the frequencies of 1640~1650 cm^{-1} were ascribed to the random-coil structure, absorption bands in the frequency range of 1650~1660 cm^{-1} were identified as alpha-helix structure, and peaks above 1660 cm^{-1} were ascribed to β-turns [16, 29, 33]. Fourier Self-Deconvolution (FSD) of the infrared spectra covering the amide I region (1595~1705 cm^{-1}) was performed with Opus 5.0 software from Bruker Optics Corp. (Billerica MA) [16]. Using a high pass filter, the broad and indistinct amide I bands were narrowed by FSD to provide a deconvoluted spectrum with better peak resolution [16, 18]. Finally, the deconvoluted amide I spectra were area-normalized, and the relative areas of the single bands were curve-fitted and used to determine the fraction of the secondary structural contents in the silk-tropoelastin composites.

Atomic Force Microscopy (AFM)

AFM imaging and roughness characterization of the protein films were performed in tapping mode on a Dimension 3100 Scanning Probe Microscope with Nanoscope III and IV controllers (Digital Instruments, Santa Barbara, CA) and equipped with rotated tapping-mode etched silicon probes (Nanodevices, Santa Barbara, CA). Silk-tropoelastin protein film samples (20~30 μm) prepared for AFM were first soaked with Milli Q-water for 20 min and dried with nitrogen, then AFM image scans of 10×10 μm were conducted in air. The roughness value R_a, representing the average distance between the surface and the mean line from recordings at each point in the height profile was calculated from each film's AFM image using Nanoscope Image Processing software.

Biomechanical strength

Mechanical Analysis (Uniaxial tensile test) was performed on an Instron 3366 (Norwood, MA, USA) testing frame equipped with a 100 N capacity load cell and Biopuls pneumatic

clamps [35]. Different silk-tropoelastin blend solutions were first cast on rectangular shape PDMS substrates and dried to make films (5 mm × 4 cm), after which they were treated with water vapor at 60°C [35] and then hydrated in 0.1 M phosphate-buffered saline (PBS) for 2 hr to reach a swelling equilibrium prior to testing. Test samples were submerged in a Biopuls temperature-controlled testing container (TM) filled with 37°C PBS. A displacement control mode with a crosshead displacement rate of 5 $mm \cdot min^{-1}$ was used and a gauge length of 15 mm. The measured width of the gauge region was multiplied by the average specimen thickness (measured by a Carrera Precision Digital LCD Caliper Micrometer) in order to convert load data to tensile stress values. The initial elastic modulus, yield stress, and tensile strength were calculated from stress/strain plots [35]. The initial elastic modulus was calculated by using a least-squares fitting between 0.05 N load and 5% strain past this initial load point [35]. The yield strength was determined by offsetting the least-squares line by 2% strain and finding the data intercept. Ultimate tensile strength was defined as the highest stress value attained during the test. Sample sets (n=6) were statistically analyzed by Student t-tests.

Isolation and culture of myoblasts (C2C12) and hMSCs

C2C12 myoblasts were obtained from the American Type Culture Collection (ATCC, Rockville, MD). Cells were initially seeded on 10 cm gelatin-coated (Sigma) culture plates (Fisher Scientific) containing 10 mL growth medium (GM) consisting of Dulbecco's modified Eagle's medium (D-MEM) (Invitrogen), 10% fetal bovine serum (FBS) (HyClone), 2 mM L-glutamate (Invitrogen), 50 units/mL penicillin-streptomycin (Invitrogen) and 1 mM sodium pyruvate (Invitrogen). The culture medium was changed every other day.

hMSCs were isolated and expanded [36]. Bone marrow aspirates (25 ml, Lonza, 27 year old male, Walkersville, Inc., MD) were diluted in 75 ml PBS. The cells were separated by density gradient centrifugation. Twenty ml aliquots of bone marrow suspension were overlaid onto a poly-sucrose gradient (1077 g/cm^3, Histopaque, Sigma, St. Louis, MO) and centrifuged at 800 ×g for 30 min at room temperature. The cell pellet was resuspended in Minimum Essential Medium Eagle (α-MEM: Gibco BRL) supplemented with 10% FBS (Gibco BRL), 100 U/mL penicillin G (Gibco BRL) and 100 μg/mL streptomycin (Gibco BRL). Cell number and viability were determined using trypan blue exclusion. The resuspended cells were plated at a density of 1.5×10^5 $cells/cm^2$.

Cell response and differentiation on silk-tropoelastin films

Osteogenic medium was used with hMSC for 2 wk and consisted of α-MEM supplemented with 10% FBS, 0.1 mM nonessential amino acids, 50 μg/ml ascorbic acid-2-phosphate, 100 nM dexamethasone, 10 mM β-glycerol phosphate and 100 ng/ml BMP-2 in the presence of 100 U/ml penicillin, 100 μg/ml streptomycin, and 0.25 μg/ml fungizone. To induce differentiation from myoblasts to myotubes for 2 wk, the medium was replaced at confluence (= day 0) with differentiation medium consisting of DMEM with 2% horse serum supplementing the antibiotics. All cultured cells were evaluated with a Leica DMIL light microscope (Watzlar, Germany) and Leica Application Suite (v3.1.0) software [14].

Passage 3 hMSCs and C2C12 cells were seeded onto prewetted (α-MEM and DMEM, overnight) silk-tropoelastin films at a density of 2×10^5 cells/film. Morphology of attached cells was microscopically observed after 3 hr and floating cells were counted over 1, 3, and 6 hr. Cell proliferation on the silk substrates was also evaluated using DNA content based on the Pico Green assay (Invitrogen). Seeded cells were cultured over 1, 3, 5, and 7 days before measuring DNA content. For the Pico Green assay, samples were washed twice with PBS and subsequently incubated in 1 mL 0.1% Triton-X 100 in 1 × TE buffer for 48 hr. The

sample supernatant centrifuged for 5 min at 10,000 rpm. Subsequently, 25 μL supernatant and 75 μL TE were placed into 96-well plates and 100 μL 1:200 dilution of Quant-iT PicoGreen (Invitrogen) reagent was added to each well then read using a fluorimeter at an excitation wavelength of 480 nm and an emission wavelength of 520 nm.

Biochemical analysis

Cell cultured silk-tropoelastin films (N=4) were extracted twice with 0.5 ml 5% trichloroacetic acid for total calcium content. Alkaline phosphatase (ALP) activity was measured by biochemical assay from Stanbio Laboratory (Boeme, TX), based on conversion of p-nitrophenyl phosphate to p-nitrophenol, which was measured spectrophotometrically at 405 nm. Calcium content was determined by a colorimetric assay using ortho-cresolphthalein complexone (OCPC, Stanbio Laboratory, Boeme, TX). The calcium complex was measured spectrophotometrically at 575 nm.

Histochemical staining for osteogenesis

To analyze the osteogenic differentiation of hMSCs, alkaline phosphatase (ALP) staining was assessed following histochemical staining (Sigma). Cells were incubated with alkaline-mixture (2.4 mg fast violet B salt and 0.4 mL naphthol AS-MX phosphate alkaline solutionin 9.6 mL distilled water) for 45 min at room temperature in a dark room. For alizarin red staining, cells were fixed in 4% formaldehyde after washing twice with PBS. After two times washing with phosphate buffered saline (PBS), cells were stained with 40 mM alizarin red S (pH 4.2) for 10 min. All stained cells were observed by with a Leica DMIL light microscope and Leica Application Suite (v3.1.0) software after two times washing with PBS.

Immunofluorescent staining for ECM

Cell culture medium was gently removed and cell cultured films were washed twice with PBS (pH 7.4). Subsequently, the samples were fixed for 10 min at room temperature using 4% paraformaldehyde solution then washed 3 times with PBS. The cells were permeabilized with PBS (pH 7.4) containing 0.2% Triton X-100 for 10 min, and blocked with PBS (pH 7.4) containing 1% BSA for 30 min. After diluting, 1 mL was placed onto each sample for 30 min with two subsequent PBS rinses. Primary antibodies for Myosin 1d (Myo1d), bone sialoprotein (BSP), and osteopontin (OP) were diluted from their respective stock solutions to 5–10 μg/mL concentrations in PBS. 250 μL antibody solution was placed onto each sample in 24 well plates and incubated at 4°C overnight. The samples were then washed 3 times with PBS and stained using fluorescein isothiocyanate (FITC) as secondary antibody, in which a 10 μg/mL dilution was prepared. A 250 μL aliquot of secondary antibody solution was added to each sample for 30 min with 2 subsequent PBS rinses. All antibodies were purchased from Abcam, Inc.

Confocal microscopy was carried out to examine cytoskeleton and ECM synthesis. The middle z-section images of cells were taken with a Leica TCS SP2 AOBS confocal microscope equipped with 488 nm argon and 543 nm He/Ne lasers. FITC secondary antibody excitations were at 488 nm, and collected emission between 500 and 550 nm.

Real-time PCR

One ml Trizol was added in the cell cultured films (N=4 per group). Films were incubated for 20 min at room temperature. The supernatant in each case was transferred to a new tube for RNA purification. Chloroform (200 ml) was added and incubated for 5 min at room temperature. Tubes were centrifuged at 12,000 g for 15 min and the upper aqueous phase was transferred to a new tube. One volume of 70% ethanol (v/v) was added and applied to

an RNeasy mini spin column (Qiagen). The RNA was washed, eluted aand reverse transcribed into cDNA using oligo (dT)-selection according to the manufacturer's protocol (High Capacity cDNA Archive Kit, Applied Biosystems). Myosin-1d (Myo1d), ALP, BSP and OP levels were quantified using z Mx3000 Quantitative Real Time PCR system (Stratagene). All data analysis employed the Mx3500 software based on fluorescence intensity values after normalization with an internal reference dye and baseline correction. Differences of gene expression were generate by using comparative Ct method (Ct [delta] [delta] Ct comparison). PCR reaction conditions were 2 min at 50°C, 10 min at 95°C, and then 50 cycles at 95°C for 15 s, and 1 min at 60°C. The data were normalized to the expression of the housekeeping gene, glyceraldehyde-3-phosphate-dehydrogenase (GAPDH) within the linear range of amplification and differences[14]. The GAPDH probe was labeled at the 5' end with fluorescent dye VIC and with the quencher dye TAMRA at the 3' end.

Statistical analysis

Statistical differences were determined using a Mann-Whitney U test (Independent t-test, SPSS). A statistical significance was assigned as *$p<0.05$, **$p<0.01$ and ***$p<0.001$, respectively.

Results and Discussion

Physical Crosslinking of silk-tropoelastin films

FTIR analysis was performed to understand the structures of silk, tropoelastin, and their different blends before and after physical crosslinking. Figure 1(a) and (b) show typical FTIR absorbance spectra of pure soluble tropoelastin films (SE0), and soluble silk films (SE100) before the crosslinking treatments, respectively, for the Amide I (1700-1600 cm^{-1}) and Amide II (1600-1500 cm^{-1}) regions. According to previous studies [16, 34, 35], the Amide I region directly reveals the secondary structure of the proteins [16], and the Amide II can indicate the changes in protein side chains [19]. In addition, through curve fitting of Fourier self-deconvoluted (FSD) spectra [16] in the Amide I region, the percentage of secondary structures in the different silk-tropoelastin samples can be quantified [34]. In general, untreated tropoelastin films (Fig 1(a)) show a typical alpha-helices (A) dominated structure with a peak centered at 1653 cm^{-1}, while 34% of beta-turn (1660 to 1690 cm^{-1}) structures can be obtained in these soluble films. In contrast, untreated silk films (Fig 1(b)) tend to have more structural contributions from random coils (R), with a maximum peak position centered at 1642 cm^{-1} in Amide I.

To induce insolubility of the silk-tropoelastin samples, temperature-controlled water vapor annealing (TCWVA), was used to control and crosslink structures through physical water vapor annealing at different temperatures (4°C~100°C) [35]. Under these conditions, silk materials can be prepared with control of crystalline content from the lowest beta sheet value (~14%) at 4°C, to the highest ~60% at 100°C, which covers all other crosslinking methods for the fabrication of insoluble silk materials [35]. This controlled annealing step is due to the plasticization of water vapor molecules into the protein chain networks to significantly reduce the original glass transition temperature of the protein system (for pure silk-178°C [16, 34], for pure tropoelastin-190°C [34]) to below the annealing temperatures (0~100°C). The additional water vapor molecules at different temperatures can transfer variable thermal energy into the protein-bound water system, and induce self-assembly of protein chains to become insoluble stacked crystals [35].

In the present study, this technique was evaluated to determine utility for physical crosslinking of pure tropoelastin (SE0) protein at different annealing temperatures. The

water vapor annealing of soluble tropoelastin films in the lower temperature region, especially below the coacervation temperature of tropoelastin around 37°C [37, 38], did not significantly induce physical crosslinking. FTIR results show that tropoelastin remained with alpha-helix and random coil dominated conformations centered around 1645 to 1655 cm^{-1}. However, once the vapor annealing temperature increased above the tropoelastin coacervation temperature region (37~45°C) [37], the structural transition of tropoelastin became significant, from alpha-helix dominated conformations to a mixed structure with a large content of beta sheet crystals. Figure 1(c) shows a typical FTIR spectrum of tropoelastin films water-annealed at 60°C for 12h. A strong beta-sheet shoulder around 1630 cm^{-1} in the Amide I region increased after annealing, compared with the untreated sample in Fig 1(a). The side-chain sensitive absorbance in the Amide II region also shifted to a lower wavenumber, indicating the packing of the dense beta-sheet crystals during the vapor annealing process [19]. Moreover, the tropoelastin samples became insoluble after this process, which indicated this physical crosslinking technique worked well for tropoelastin, by inducing insoluble beta-sheet crystals as crosslinkers in the protein network.

The crosslinking effects of the 60°C water vapor annealing for the silk fibroin-tropoelastin blends were studied by FTIR. Figure 1 (d)-(g) show the typical FTIR spectra of 60°C water annealed blend samples with different mixing ratios, (d) SE50, (e) SE75, (f) SE90, and (g) SE100. Initially, all untreated samples were in the non-crystalline state, as described previously, and there was no significant peak observed in the main wavenumber region of beta-sheet crystal (1600~1640 cm^{-1}) [16]. After 12h annealing in a 60°C water vapor environment, the beta-sheet crystal peak gradually appeared in all samples, centered at 1626 cm^{-1}. The random coil peaks (1640~1649 cm^{-1}) and the alpha-helix peak (centered at 1650 cm^{-1}) decreased simultaneously. With the decrease of silk fibroin content in the composite system, water-annealed bulk films can not maintain original shape easily after soaking in PBS solution. For example, the pure tropoelastin films shrink into a fiber-like morphology due to their low rigidity [1-3], even with some beta-sheet structure. Therefore, considering future biomechanical applications of these blends, especially the potential to be designed as 3-D tissue extracellular matrix, we selected not to continue further with the tropoelastin dominated samples, such as SE25 and SE10, which often have obvious low elastic modules and short term stability. These samples may find utility in other biomaterial carriers and will be pursued separately.

Surface roughness

The surface features of the different silk-tropoelastin films after 60°C water annealing were assessed by AFM. Figure 2(a)-(e) show the AFM 3-D topography of the 60°C water annealed films for (a) SE100 (pure silk), (b) SE90, (c) SE75, (d) SE50, and (e) SE0 (pure tropoelastin), as the control. Figure 2(f) summarizes the surface roughness values. For water vapor crosslinked pure silk (Fig 2(a)), the R_a was 41.4±2.6 nm. At 10 wt% tropoelastin (SE90, Fig 2(b)), the film showed a smoother surface with a lower roughness of 22.8±0.7 nm ($p^{*}<0.05$). With increasing tropoelastin content (SE75, SE50), film roughness increased dramatically, at 73±5.7 nm for SE75 and the highest at 90.9±12.3 nm for SE90 ($p^{**}<0.01$ compared with SE90 and SE100). Water annealed pure tropoelastin (SE0), as a control, had a surface roughness of 23.8±2.1 nm, close to that of SE90. Surface roughness is usually related to the properties of material and the post-treatments of material surfaces. In this case, the same water annealing treatment was performed on all samples, thus the differences were likely due to the interactions between the material components. Silk fibroin is a long chain protein containing a heavy chain and a light chain, with a total molecular weight ~420 kDa, and a -36 side chain net charge at pH 7 [39]. Tropoelastin has a molecular weight of ~60 kDa, with a positive +37 net charge at neutral pH [1-3]. When long chain silk is mixed with short chain tropoelastin using a mass ratio of 90:10 (SE90), their molar ratio are very close

to 1:1 with a total neutral charge, indicating that the same number of silk chains interacts with tropoelastin chains. Therefore, its surface energy tends to be the lowest in this blend group, which resulted in the lowest surface roughness. Different high-density micro/nano-porous structures are found in the blend samples of SE75 and SE50 [34], which could explain the substantial increase in surface roughness.

Mechanical properties

Tensile stress-strain tests for the different 60°C water vapor annealed silk-tropoelstin films were performed at 37°C in a PBS hydrated environment. Figure 3(a, b, c) show the calculated values for modulus of elasticity, yield stress and tensile strength from the sample sets (each n≥6) of crosslinked SE100, SE90, SE75, and SE50. Silk-tropoelastin samples exhibited variable force vs. axial strain profiles with changes in the mixing ratio. In general, an increase in tropoelastin content resulted in lower strain values at a defined stress; thus SE100 samples (pure silk) had the highest stiffness (or elastic modulus) around 27 MPa, which gradually decreased with an increase in tropoelastin content. The SE50 sample displayed a lower elastic modulus of about 5MPa, which is close to the typical stiffness region of soft tissues (0.1 kPa~1 MPa) [40]. In contrast, initial tensile stress-strain tests showed that 60°C water-annealed pure tropoelastin (SE0) had a low Young's modulus of 0.54±0.09 MPa, with a yield stress around 0.176±0.045 MPa, which are significantly lower than the values from SE50. The tensile strength of water-annealed tropoelastin was reduced to 572±32 kPa, resulting in unstable material shape in 37°C PBS solution. This result was expected as it has been previously demonstrated by FTIR that silk films induce greater beta-sheet content than do pure tropoelastin films (SE0), while increased beta-sheet content enhances stiffness [35]. The data revealed that crosslinked silk films (SE100) exhibit significantly ($p^*<0.05$) more modulus of elasticity, tensile strength, and yield stress, when compared with the SE50 films. On this basis, the results indicated that the mixing ratio of silk and tropoelastin could be used directly to manipulate the mechanical properties of the insoluble materials to assess their influence on cellular responses.

Cells response on silk-tropoelasin substrates

The silk-tropoelastin films were placed in 12 well plates, seeded with C2C12s or hMSCs or and cultured *in vitro*. In cell attachment assays, the films did not show a statistical difference after 6 hr of myoblast (C2C12) cell seeding, while the SE50 showed 20% less attachment than the SE 100 after 1hr (Fig. 4a). In contrast, hMSCs on SE50 showed 8% higher cell attachment compared to SE90 and SE100 ($p^*<0.05$). However, SE50 did not show a statistical difference compared with SE75 after 6 hr (Fig. 4b).

The DNA content was determined for cells grown on silk or silk-tropoelastin surfaces over a seven-day period to examine the effect of tropoelastin on cell proliferation. Cell proliferation rate of C2C12s on SE90 by day 7 was the highest among all groups ($p^*<0.05$). In particular, SE75 and SE50 exhibited lower but not significant DNA content than SE100 over 5 and 7 days in culture (Fig. 5a). However, hMSC proliferation on tropoelastin blends showed significantly ($p^*<0.05$) higher DNA content than SE100 at day 7, even though DNA content increased over time on all the films. Tropoelastin concentration did not affect the amount of hMSC proliferation. Cells on pure silk films had a more aggregated morphology compared to those on the tropoelastin blends (Fig. 5b) which could mean that blended tropoelastin enhanced hMSC proliferation on silk surfaces, while higher concentrations of tropoelastin delayed C2C12 proliferation on silk surfaces.

Myogenesis of C2C12

Myogenic differentiation was demonstrated by the expression of the contractile protein myosin. By immunohistochemistry, higher expression of Myo1d was exhibited on SE90

compared to SE100 and SE75, while SE50 has the lowest average expression after 2 wk (Fig. 6a). After 2 wk, SE90 exhibited 3 times higher myogenic transcript expression than SE75 and SE50 ($p^{***}<0.001$). In addition, SE75 and SE50 showed lower average expression ($p^{*}<0.05$) than the control SE 100 (Fig. 6b), consistent with the immunostaining reported above.

Osteogenesis of hMSC

Osteogenic differentiation of hMSCs on each film type was evaluated by biochemical analysis, immunostaining and transcript levels. ALP activity as a marker of early osteoblastic differentiation displayed activity on all films by day 14 and SE50 was significantly ($p^{*}<0.05$) increased when compared to the levels of the other samples. (Fig. 7 a, c). Calcium staining and dissolution comfirmed mineralized matrix after 2 wk on SE50 with a deeper color than that on SE100 indicative of mineralized matrix deposition. Increased calcium deposition was observed with increased tropoelasin in silk films. Calcium deposition on SE50 was 2.5-, 2- and 1.3 –fold higher than on SE 100, SE 90 and SE 75, respectively (Fig. 7 b, d).

BSP and OP were stained to examine the progress of osteogenesis,-. While all samples showed synthesized BSP on the films, some notable differences were apparent in the expression levels between SE50 and SE100 (Fig. 8a). In addition, OP was widely distributed in tropoelastin blended silk films compared to SE100. In particular, SE50 exhibited stronger staining at 2 wk than SE100 (Fig. 8b). To further support the staining, transcript levels of osteogenic markers colIα1, BSP, OP and Cbfα1 were analyzed by RT-PCR. Col Iα1 transcript level in the SE50 was more highly expressed at 2 wk than SE100 ($p^{*}<0.01$). At this time point, the mRNA levels of BSP and OP were higher overall in tropoelastin blend silk films than in pure films. In particular, the mRNA level of Cbfα1 on SE 50 was significantly ($p^{***}<0.001$) higher than that on SE100. Statistical differences were observed in mRNA levels of all genes between the absence and presence of tropoelastin, except for SE 75which showed no significant difference from SE90 (Fig. 8c).

Mechanism of stem cell response to silk-tropoelastin films

Cell functions can be regulated by extracellular stimuli, including adhesive factors and soluble factors that bind to cell-surface receptors [40-65]. Three factors from the extracellular matrix: (1) chemical properties (such as the biomatrix composition, crosslinking chemistry, surface charges, and integrin receptor sites on the materials) [41-45, 65], (2) the topographical features of the interfaces (surface energy, surface morphology, surface roughness) [51-56, 58, 59, 61, 63, 64], and (3) mechanical properties of the extracellular materials (elastic modulus or rigidity, elasticity ratio, dynamic mechanical vibration) [40, 46-50, 57, 60, 62] were recently demonstrated to play important roles in various cellular processes, including cell attachment, migration, proliferation, and stem cell differentiation [40-65]. These three factors on adhesive substrates can work synergistically to regulate cell responses at early time points at the interface. Therefore, alterations in one or more of these material properties may result in long-term changes in cellular responses, including different phenotype-specific gene expression and functional differentiation.

Tropoelastin and silk are native proteins but with different biochemical properties. Cell adhesion to human tropoelastin is mediated via the C-terminal region and at least integrin αvβ3 [41-43]. In contrast, mediation of the interactions of silk with cells (especially bone cells) [44, 45] are less specific than with tropoelastin, with some data to show that silk fibroin contains RGY and RGV, which results in binding of ITGA5 (integrin alpha-5) [44]. In light of these previous findings, tropoelastin, as a native human protein with cell signaling capability, should be more favorable for initial cell interactions especially human cells such

as hMSCs. A blend of elasticity, surface roughness and cell binding is likely to contribute to the observed combination of proliferation and ostegenesis of hMSCs on silk-tropoelastin surfaces with increased tropoelastin content.

Recent evidence [40, 46-50, 57, 60, 62] suggests that mechanical properties of the extracellular matrix, particularly stiffness, can mediate cell proliferation, signaling, and differentiation. Stiff substrates can promote the formation of cytoskeletal organization and focal adhesions for some cell cultures, while soft substrates are not favorable for their anchoring, spreading or proliferation. Ren *et al*. [60] investigated the stiffness of thin multilayer poly (L-lysine)/hyaluronan (PLL/HA) films on C2C12 differentiation. Film stiffness modulated their initial adhesion and proliferation but also differentiation into myotubes. Soft films allowed differentiation for only a few days and the myotubes were very thick and short [60]. In contrast, on stiff films (stiffness >320 kPa), clumping cells with elongated and thin striated myotubes were found for up to 2 wk [60]. In addition, Gilmore *et al*. [54] found that enhanced myofiber formation correlates with films that show lower roughness, by studying adhesion and differentiation of C2C12s and myoblasts on polypyrrole related films. In contrast, Charest e*t al*. [56] analyzed the alignment and differentiation of C2C12 cells on surfaces with different micro-topographical patterns. The patterns strongly influenced cellular alignment but did not affect cell density or the expression of differentiation marker proteins, indicating that micro/nano-scale patterns only modulate alignment, but not C2C12 cell density or differentiation. These results suggest that C2C12 muscle cell are sensitive to the mechanical properties and average surface roughness of materials, but are relatively insensitive to specific topographical micro/nano-patterns. A combination of low surface roughness and high surface stiffness is favorable for proliferation and differentiation of C2C12 cells. This phenomenon was demonstrated by SE90 and SE100, which displayed the lowest (R_a~22.8 nm), and the second lowest surface roughness (R_a~41.4 nm) with relatively high elastic modulus (20~28MPa). In addition, although silk/tropoelastin systems have different micro/nano porous patterns on the surface (especially for SE75 and SE50 [34]), these features had limited impact on the proliferation and differentiation of C2C12 cells. However, with an increase of tropoelastin content in the silk-tropoelastin systems from SE90 to SE50, the stiffness of the films decreased significantly (~5MPa for SE50) and in turn roughness increased (R_a~90.9 nm), correlating with a reduction in the number of C2C12 cells and delayed differentiation compared with SE90. Therefore, surface average roughness and material stiffness together appeared to be the dominant factors that affected the behavior of C2C12 cells on the silk/tropoelastin films. On this basis, SE90 provided the best extracellular environment for the proliferation and myo1d protein and gene expression in C2C12 culture [55, 56] in this study.

The behavior of hMSCs differs from C2C12 cells, where hMSCs prefer rougher surfaces [58, 59, 61, 63-65]. Balloni et al. [59] examined changes in hMSC morphology, proliferation, and gene expression after growth on machined smooth titanium surfaces and dual acid-etched titanium surfaces with a higher surface roughness. They found that Osx, BMP-2, and Runx2, the three osteogenic factors that induce progressive differentiation of mesenchymal cells into osteoblasts, were more highly expressed on the rougher surface elevated collagen and ALP transcripts correlated with the increases [59]. According to this model, a higher surface roughness (such as SE75 and SE50 in the present study) would stimulate the expression of markers of osteoblastic phenotype. Mendonca et al. [64] showed that surface nanoscale features enhanced hMSC gene expression related to osteoblast differentiation, where hMSCs showed increased OSX and BSP mRNA [64].

hMSC cells *in vivo* typically sense stiffness on the order of 0.1-800 kPa [40, 47]. They increase spreading with substrate rigidity to a maximum attachment on 25 kPa substrates [40, 47]. Cells on the softest (~0.1 kPa) gels exhibit branching and filopodia formation with

less osteoblastic polygonal morphology and osteogenic markers [40, 47]. However, the elastic modulus region of all silk-tropoelastin substrates studied here (around 1~30 MPa) are too stiff to mediate this effect. SE50 had the lowest elastic modulus of ~5MPa, which is still above 0.1-800 kPa. Interestingly, the softest SE50 in the group tended to support significantly higher transcript levels and cell-matrix interactions, suggesting that either lower elastic modulus in the region of 1~30MPa might oppositely promote the proliferation and differentiation of hMSCs, or a bulk stiffness region close to 0.1-800 kPa could favor better osteogenic differentiation of hMSCs [40, 47], or other parameters such as biochemical properties (human tropoelastin componets can mediate hMSC adhesion via integrins) play a dominate role for this cell type. This phenomenon is also found in water-annealed pure silk films at different temperatures [35], in which lower stiffness (Young's modulus) samples enhanced proliferation and cell viability of hMSCs (elastic modulus region: 10~100MPa). A similar case was also found on a 2HEMA-PEGDMA system (2-hydroxyethyl methacrylate and poly(ethylene glycol) dimethacrylate) [66], where human MG63 pre-osteoblast cells differentiated more on the less stiff substrates (around 10MPa) [66]. In summary, the chemical properties of the substrates, such as the human tropoelastin content, and the surface features, including both roughness and micro/nano scale patterns, could be the most important parameters that affect the proliferation and differentiation of hMSCs on silk-tropoelastin blends.

Conclusions

The interactions of silk-tropoelastin biomaterials with C2C12 cells and hMSCs was assessed for attachment, proliferation and differentiation. Insoluble silk-tropoealstin matrices were prepared by a physical crosslinking method through temperature-controlled water vapor annealing. Beta-sheet crystals were induced in silk and tropoelastin protein chains to form the insoluble crosslinkers in the materials. Surface roughness and mechanical properties were controlled in this process. A combination of low surface roughness and high stiffness of the substrate appeared to be the most favorable for proliferation and myogenic-differentiation of C2C12 cells, while the impact of topographical micro/nanoscale patterns and the protein material composition was relatively less important to the responses of this cell type. In contrast, hMSCs demonstrated a preference for a higher content of human tropoelastin, together with higher surface roughness and stronger micro/nano scale surface patterns, which collectively enhanced the proliferation and osteogenic differentiation of hMSCs on the silk-tropoelastin blends. The significantly different cell responses indicated that silk-tropoelastin blends can serve to regulate and manipulate stem cell growth and tissue formation. Technical advances in the design of this material system with controlled properties, including protein composition, internal structure, surface feature and roughness, and mechanical properties indicate the value of this protein interface in applied cell biology.

Acknowledgments

The authors thank the NIH P41 Tissue Engineering Resource Center (P41 EB002520) and the Air Force Office of Scientific Research for support of this research. ASW acknowledges grant support from the Australian Research Council, the National Health and Medical Research Council and the Defence Health Foundation.

References

1. Almine J, Bax D, Mithieux S, Nivison-Smith L, Rnjak J, Waterhouse A, et al. Elastin-based materials. Chem Soc Rev. 2010; 39:3371–3379. [PubMed: 20449520]
2. Vrhovski B, Weiss AS. Biochemistry of tropoelastin. Eur J Biochem. 1998; 258:1–18. [PubMed: 9851686]

3. Baldock C, Oberhauser AF, Ma L, Lammie D, Siegler V, Mithieuxd SM, et al. Shape of tropoelastin, the highly extensible protein that controls human tissue elasticity. Proc Natl Acad Sci U S A. 2011; 108:4322–4327. [PubMed: 21368178]
4. Yu J, Urban JP. The elastic network of articular cartilage: an immunohistochemical study of elastin fibres and microfibrils. J Anat. 2010; 216:533–541. [PubMed: 20148992]
5. Wise SG, Mithieux SM, Weiss AS. Engineered tropoelastin and elastin-based biomaterials. Adv Protein Chem Struct Biol. 2009; 78:1–24. [PubMed: 20663482]
6. Urry DW. Physical chemistry of biological free energy transduction as demonstrated by elastic protein-based polymers. J Phys Chem B. 1997; 101:11007–11028.
7. Ifkovits JL, Devlin JJ, Eng G, Martens TP, Vunjak-Novakovic G, Burdick JA. Biodegradable fibrous scaffolds with tunable properties formed from photo-cross-linkable poly(glycerol sebacate). ACS Appl Mater Interfaces. 2009; 1:1878–1886. [PubMed: 20160937]
8. Teng WB, Cappello J, Wu XY. Recombinant silk-elastin like protein polymer displays elasticity comparable to elastin. Biomacromolecules. 2009; 10:3028–3036. [PubMed: 19788307]
9. Omenetto FG, Kaplan DL. New opportunities for an ancient material. Science. 2010; 329:528–531. [PubMed: 20671180]
10. Omenetto FG, Kaplan DL. A new route for silk. Nat Photonics. 2008; 2:641–643.
11. Vepari C, Kaplan DL. Silk as a biomaterial. Prog Polym Sci. 2007; 32:991–1007. [PubMed: 19543442]
12. Wang Y, Kim HJ, Vunjak-Novakovic G, Kaplan DL. Stem cell-based tissue engineering with silk biomaterials. Biomaterials. 2006; 27:6064–6082. [PubMed: 16890988]
13. Meinel L, Hofmann S, Karageorgiou V, Kirker-Head C, McCool J, Gronwicz G, et al. Inflammatory responses to silk films in vitro and in vivo. Biomaterials. 2005; 26:147–155. [PubMed: 15207461]
14. Park S, Gil ES, Shi H, Kim HJ, Lee K, Kaplan DL. Relationships between degradability of silk scaffolds and osteogenesis. Biomaterials. 2010; 31:6162–6172. [PubMed: 20546890]
15. Gil ES, Mandal BB, Park S, Marchant JK, Omenetto FG, Kaplan DL. Helicoidal multi-lamellar features of RGD-functionalized silk biomaterials for corneal tissue engineering. Biomaterials. 2010; 31:8953–8963. [PubMed: 20801503]
16. Hu X, Kaplan D, Cebe P. Determining beta-sheet crystallinity in fibrous proteins by thermal analysis and infrared spectroscopy. Macromolecules. 2006; 39:6161–6170.
17. Kim UJ, Park J, Kim HJ, Wada M, Kaplan DL. Three-dimensional aqueous-derived biomaterial scaffolds from silk fibroin. Biomaterials. 2005; 26:2775–2785. [PubMed: 15585282]
18. Hu X, Lu Q, Sun L, Cebe P, Wang X, Zhang X, et al. Biomaterials from ultrasonication-induced Silk fibroin–hyaluronic acid hydrogels. Biomacromolecules. 2010; 11:3178–3188.
19. Hu X, Kaplan D, Cebe P. Dynamic protein-water relationships during beta-sheet formation. Macromolecules. 2008; 41:3939–3948.
20. Motta A, Maniglio D, Migliaresi C, Kim HJ, Wan XY, Hu X, et al. Silk fibroin processing and thrombogenic responses. J Biomat Sci-Polym E. 2009; 20:1875–1897.
21. Wang XY, Hu X, Daley A, Rabotyagova O, Cebe P, Kaplan DL. Nanolayer biomaterial coatings of silk fibroin for controlled release. J Control Release. 2007; 121:190–199. [PubMed: 17628161]
22. Chen H, Hu X, Cebe P. Thermal properties and phase transitions in blends of nylon-6 with silk fibroin. J Therm Anal Calorim. 2008; 93:201–206.
23. Hu X, Kaplan D, Cebe P. Thermal analysis of protein-metallic ion systems. J Therm Anal Calorim. 2009; 96:827–834.
24. Lu Q, Zhang XH, Hu X, Kaplan DL. Green process to prepare silk fibroin/gelatin biomaterial scaffolds. Macromol Biosci. 2010; 10:289–298. [PubMed: 19924684]
25. Lammel AS, Hu X, Park SH, Kaplan DL, Scheibel TR. Controlling silk fibroin particle features for drug delivery. Biomaterials. 2010; 31:4583–4591. [PubMed: 20219241]
26. Kinahan ME, Filippidi E, Köster S, Hu X, Evans HM, Pfohl T, et al. Tunable silk: using microfluidics to fabricate silk fibers with controllable properties. Biomacromolecules. 2011; 12:1504–1511. [PubMed: 21438624]

27. Wang XQ, Yucel T, Lu Q, Hu X, Kaplan DL. Silk nanospheres and microspheres from silk/pva blend films for drug delivery. Biomaterials. 2010; 31:1025–1035. [PubMed: 19945157]
28. Leisk GG, Lo TJ, Yucel T, Lu Q, Kaplan DL. Electrogelation for protein adhesives. Adv Mater. 2010; 22:711–715. [PubMed: 20217775]
29. Hu X, Lu Q, Kaplan DL, Cebe P. Microphase separation controlled beta-sheet crystallization kinetics in fibrous proteins. Macromolecules. 2009; 42:2079–2087.
30. Lu Q, Hu X, Wang XQ, Kluge JA, Lu SZ, Cebe P, et al. Water-insoluble silk films with silk I structure. Acta Biomater. 2010; 6:1380–1387. [PubMed: 19874919]
31. Lu Q, Wang XQ, Hu X, Cebe P, Omenetto F, Kaplan DL. Stabilization and release of enzymes from silk films. Macromol Biosci. 2010; 10:359–368. [PubMed: 20217856]
32. Yu L, Hu X, Kaplan D, Cebe P. Dielectric relaxation spectroscopy of hydrated and dehydrated silk fibroin cast from aqueous solution. Biomacromolecules. 2010; 11:2766–2775. [PubMed: 20858000]
33. Sutherland TD, Church JS, Hu X, Huson MG, Kaplan DL, Weisman S. Single honeybee silk protein mimics properties of multi-protein silk. PLoS One. 2011; 6:e16489. [PubMed: 21311767]
34. Hu X, Wang X, Rnjak J, Weiss AS, Kaplan DL. Biomaterials derived from silk-tropoelastin protein systems. Biomaterials. 2010; 31:8121–8131. [PubMed: 20674969]
35. Hu X, Shmelev K, Sun L, Gil ES, Park SH, Cebe P, et al. Regulation of silk material structure by temperature-controlled water vapor annealing. Biomacromolecules. 2011; 12:1686–1696. [PubMed: 21425769]
36. Kim HJ, Kim UJ, Vunjak-Novakovic G, Min BH, Kaplan DL. Influence of macroporous protein scaffolds on bone tissue engineering from bone marrow stem cells. Biomaterials. 2005; 26:4442–52. [PubMed: 15701373]
37. Wise SG, Mithieux SM, Raftery MJ, Weiss AS. Specificity in the coacervation of tropoelastin: solvent exposed lysines. J Struct Biol. 2005; 149:273–281. [PubMed: 15721581]
38. Annabi N, Mithieux SM, Weiss AS, Dehghani F. Cross-linked open-pore elastic hydrogels based on tropoelastin, elastin and high pressure CO2. Biomaterials. 2010; 31:1655–1665. [PubMed: 19969349]
39. Pyda M, Hu X, Cebe P. Heat capacity of silk fibroin based on the vibrational motion of poly(amino acid)s in the presence and absence of water. Macromolecules. 2008; 41:4786–4793.
40. Nemir S, West JL. Synthetic materials in the study of cell response to substrate rigidity. Ann Biomed Eng. 2010; 38:2–20. [PubMed: 19816774]
41. Bax DV, Rodgers UR, Bilek MM, Weiss AS. Cell adhesion to tropoelastin is mediated via the C-terminal GRKRK motif and integrin alphaVbeta3. J Biol Chem. 2009; 284:28616–28623. [PubMed: 19617625]
42. Taddese S, Weiss AS, Jahreis G, Neubert RHH, Schmelzer CEH. In vitro degradation of human tropoelastin by MMP-12 and the generation of matrikines from domain 24. Matrix Biol. 2009; 28:84–91. [PubMed: 19144321]
43. Getie M, Schmelzer CE, Neubert RH. Characterization of peptides resulting from digestion of human skin elastin with elastase. Proteins. 2005; 61:649–657. [PubMed: 16161116]
44. Sengupta S, Park SH, Seok GE, Patel A, Numata K, Lu CL, et al. Quantifying osteogenic cell degradation of silk biomaterials. Biomacromolecules. 2010; 11:3592–3599. [PubMed: 21105641]
45. Horan RL, Antle K, Collette AL, Wang Y, Huang J, Moreau JE, et al. In vitro degradation of silk fibroin. Biomaterials. 2005; 26:3385–3393. [PubMed: 15621227]
46. Holst J, Watson S, Lord MS, Eamegdool SS, Bax DV, Nivison-Smith LB, et al. Substrate elasticity provides mechanical signals for the expansion of hemopoietic stem and progenitor cells. Nat Biotechnol. 2010; 28:1123–1128. [PubMed: 20890282]
47. Engler AJ, Sen S, Sweeney HL, Discher DE. Matrix elasticity directs stem cell lineage specification. Cell. 2006; 126:677–689. [PubMed: 16923388]
48. Rowlands AS, George PA, Cooper-White JJ. Directing osteogenic and myogenic differentiation of MSCs: interplay of stiffness and adhesive ligand presentation. Am J Physiol Cell Physiol. 2008; 295:1037–1044.

49. Wells SM, Walter EJ. Changes in the mechanical properties and residual strain of elastic tissue in the developing fetal aorta. Annals Biomedical Eng. 2010; 38:345–356.
50. Hamilton DW, Maul TM, Vorp DA. Characterization of the response of bone marrow-derived progenitor cells to cyclic strain: implications for vascular tissue-engineering applications. Tissue Eng. 2004; 10:361–369. [PubMed: 15165453]
51. Folkman J, Moscona A. Role of cell shape in growth control. Nature. 1978; 273:345–349. [PubMed: 661946]
52. Chung TW, Liu DZ, Wang SY, Wang SS. Enhancement of the growth of human endothelial cells by surface roughness at nanometerscale. Biomaterials. 2003; 24:4655–4661. [PubMed: 12951008]
53. Boyan BD, Lossdörfer S, Wang L, Zhao G, Lohmann CH, Cochran DL, et al. Osteoblasts generate an osteogenic microenvironment when grown on surfaces with rough microtopographies. Eur Cell Mater. 2003; 6:22–27. [PubMed: 14577052]
54. Gilmore KJ, Kita M, Han Y, Gelmi A, Higgins MJ, Moulton SE, et al. Skeletal muscle cell proliferation and differentiation on polypyrrole substrates doped with extracellular matrix components. Biomaterials. 2009; 30:5292–5304. [PubMed: 19643473]
55. McKinnell IW, Ishibashi J, Le Grand F, Punch VG, Addicks GC, Greenblatt JF, et al. Pax7 activates myogenic genes by recruitment of a histone methyltransferase complex. Nat Cell Biol. 2008; 10:77–84. [PubMed: 18066051]
56. Charest JL, García AJ, King WP. Myoblast alignment and differentiation on cell culture substrates with microscale topography and model chemistries. Biomaterials. 2007; 28:2202–2210. [PubMed: 17267031]
57. Engler AJ, Griffin MA, Sen S, Bönnemann CG, Sweeney HL, Discher DE. Myotubes differentiate optimally on substrates with tissue-like stiffness: pathological implications for soft or stiff microenvironments. J Cell Biol. 2004; 166:877–887. [PubMed: 15364962]
58. You MH, Kwak MK, Kim DH, Kim K, Levchenko A, Kim DY, et al. Synergistically enhanced osteogenic differentiation of human mesenchymal stem cells by culture on nanostructured surfaces with induction media. Biomacromolecules. 2010; 11:1856–1862. [PubMed: 20568737]
59. Balloni S, Calvi EM, Damiani F, Bistoni G, Calvitti M, Locci P, et al. Effects of titanium surface roughness on mesenchymal stem cell commitment and differentiation signaling. Int J Oral Maxillofac Implants. 2009; 24:627–635. [PubMed: 19885402]
60. Ren K, Crouzier T, Roy C, Picart C. Polyelectrolyte multilayer films of controlled stiffness modulate myoblast cell differentiation. Adv Funct Mater. 2008; 18:1378–1389. [PubMed: 18841249]
61. Lavenus S, Pilet P, Guicheux J, Weiss P, Louarn G, Layrolle P. Behaviour of mesenchymal stem cells, fibroblasts and osteoblasts on smooth surfaces. Acta Biomater. 2011; 7:1525–1534. [PubMed: 21199693]
62. Fu J, Wang YK, Yang MT, Desai RA, Yu X, Liu Z, et al. Mechanical regulation of cell function with geometrically modulated elastomeric substrates. Nat Methods. 2010; 7:733–736. [PubMed: 20676108]
63. Myllymaa S, Kaivosoja E, Myllymaa K, Sillat T, Korhonen H, Lappalainen R, et al. Adhesion, spreading and osteogenic differentiation of mesenchymal stem cells cultured on micropatterned amorphous diamond, titanium, tantalum and chromium coatings on silicon. J Mater Sci: Mater Med. 2010; 21:329–341. [PubMed: 19655235]
64. Mendonça G, Mendonça DB, Simões LG, Araújo AL, Leite ER, Duarte WR, et al. The effects of implant surface nanoscale features on osteoblastspecific gene expression. Biomaterials. 2009; 30:4053–4062. [PubMed: 19464052]
65. Phillips JE, Petrie TA, Creighton FP, García AJ. Human mesenchymal stem cell differentiation on self-assembled monolayers presenting different surface chemistries. Acta Biomater. 2010; 6:12–20. [PubMed: 19632360]
66. Smith KE, Hyzy SL, Sunwoo M, Gall KA, Schwartz Z, Boyan BD. The dependence of MG63 osteoblast responses to (meth)acrylate-based networks on chemical structure and stiffness. Biomaterials. 2010; 31:6131–6141. [PubMed: 20510445]

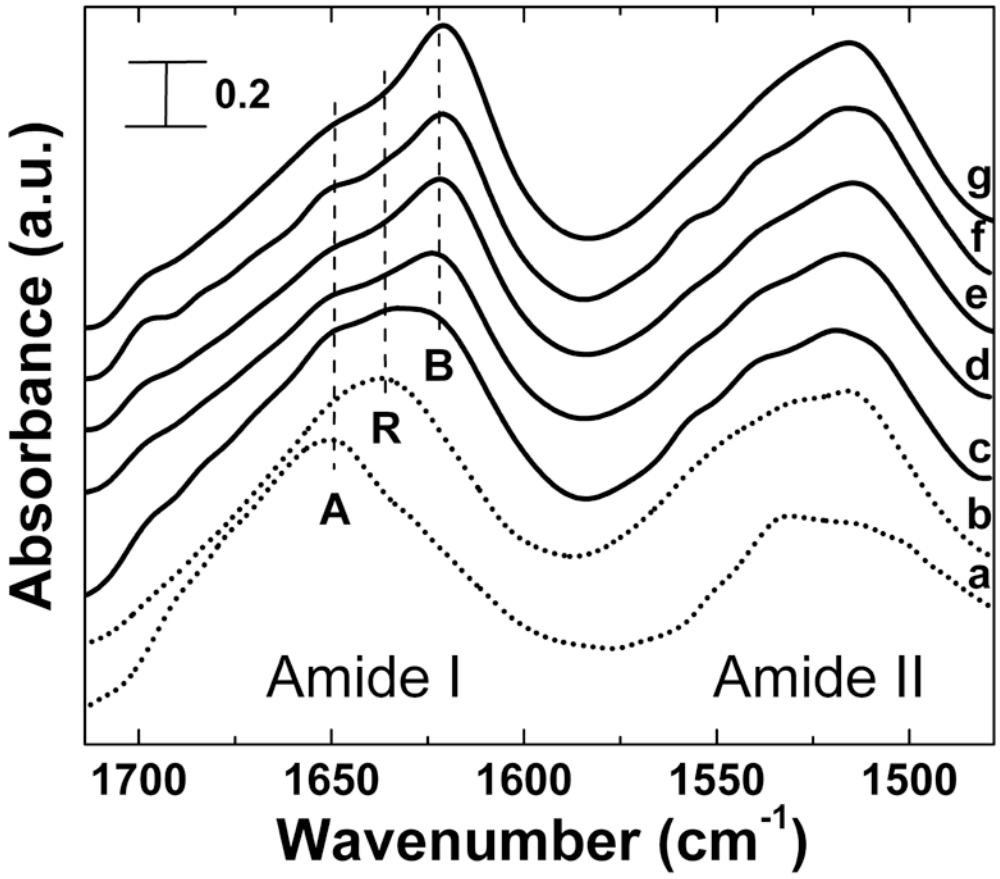

Figure 1.
FTIR absorbance spectra of (a) untreated soluble tropoelastin films, (b) untreated soluble silk films, and (c)-(g) the typical FTIR spectra of 12 hr 60°C water vapor crosslinked silk-tropoelastin films with different mixing ratios: (c) SE0 (pure tropoelastin) (d) SE50, (e) SE75, (f) SE90, and (g) SE100 (pure silk). Peaks of Amide I region indicate dominated beta-sheet (B), random coil (R), or alpha helix (A) structure.

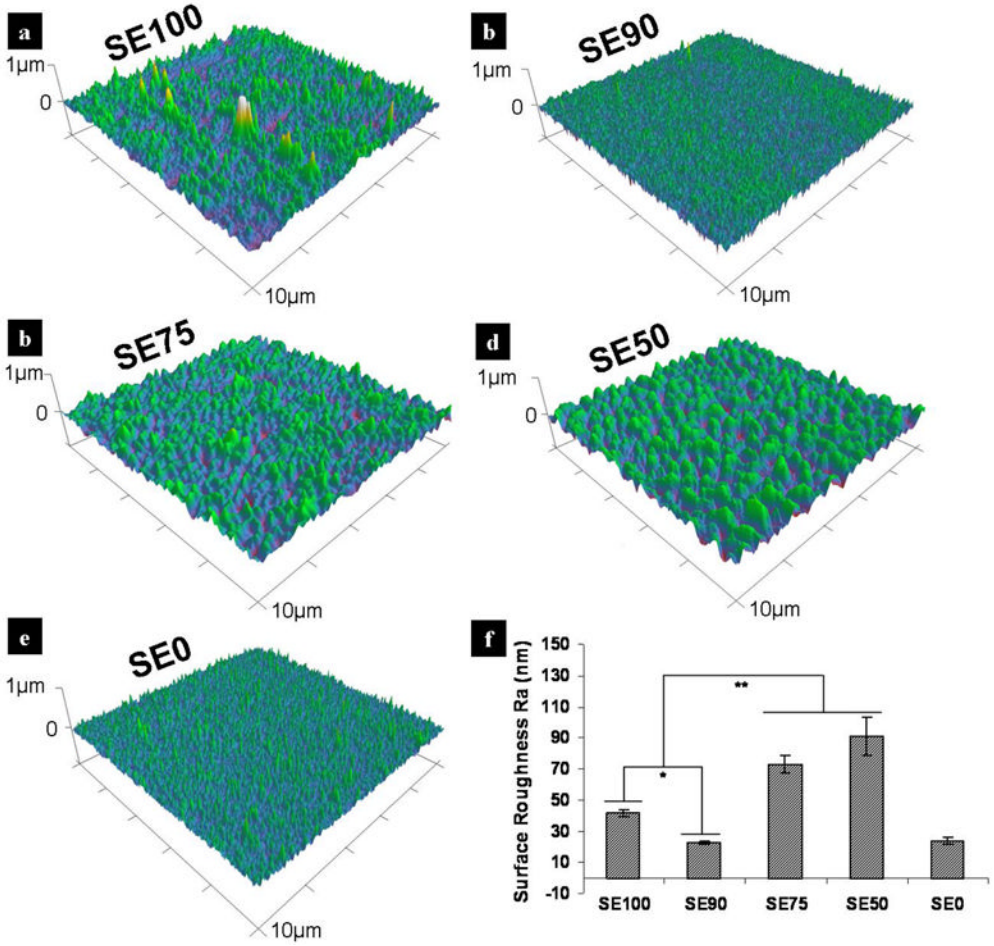

Figure 2.

AFM 3-D topography of 60°C water annealed silk-tropoelastin films (10 × 10 μm). (a) SE100 (pure silk), (b) SE90, (c) SE75, (d) SE50, and (e) SE0 (pure tropoelastin). (f) Comparison of measured R_a values. Statistically significant differences (*$p<0.05$ and **$p<0.01$).

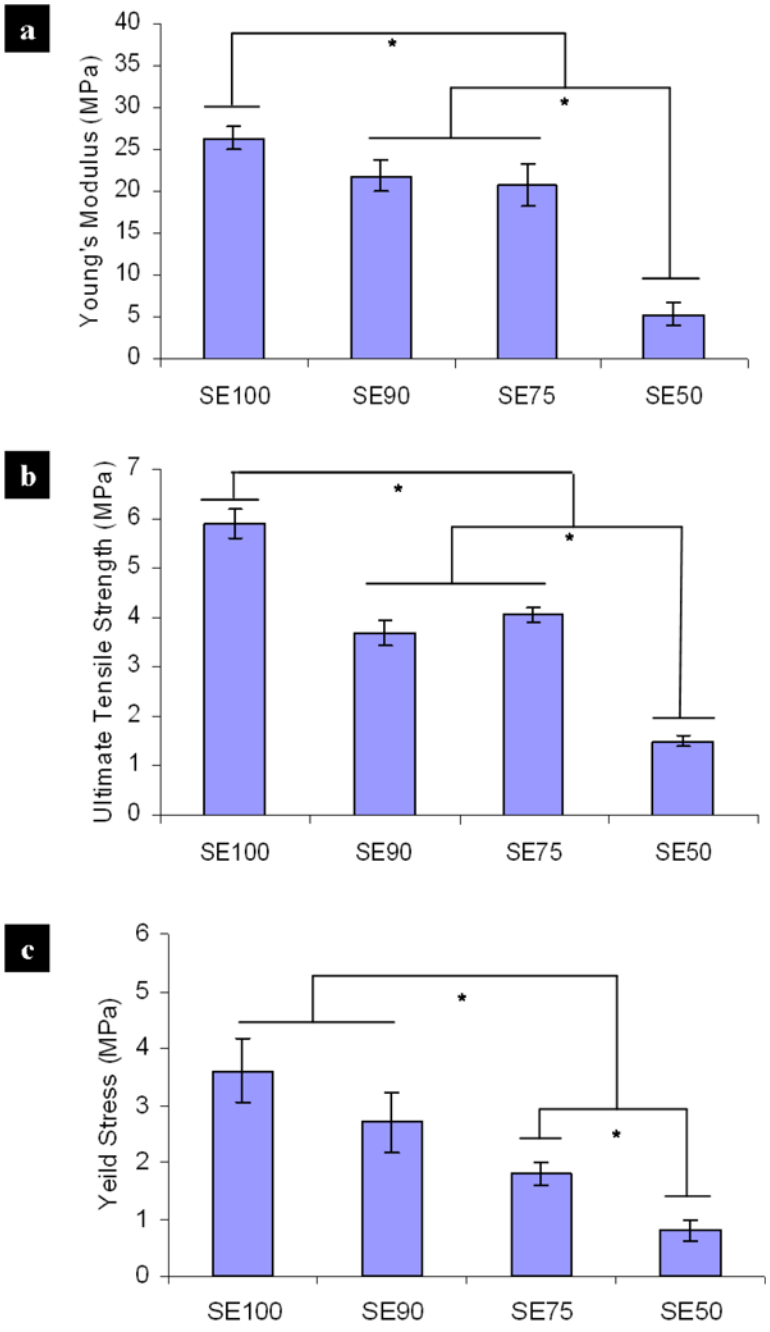

Figure 3.

Mechanical tensile stress-strain of 60°C water vapor crosslinked silk-tropoelastin films for the sample sets (each n≥6) of SE100, SE90, SE75, and SE50. Comparison of calculated values: (a) modulus of elasticity, (b) yield stress, and (c) tensile strength. Statistically significant differences (*$p<0.05$).

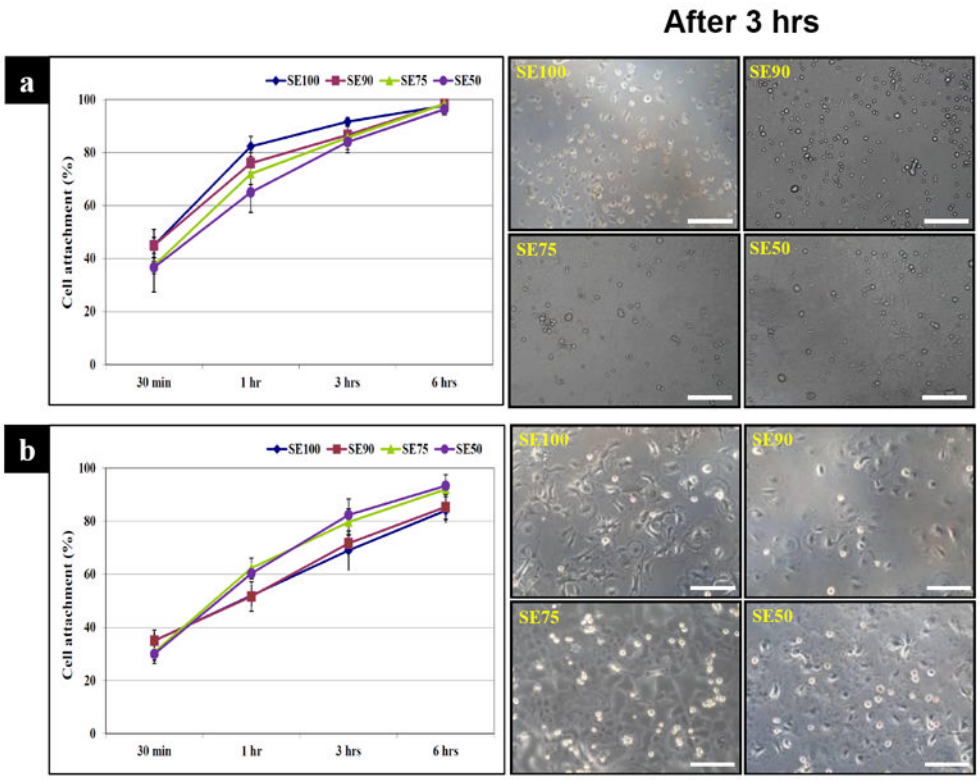

Figure 4.

Cell attachment. (a) C2C12, (b) hMSCs. C2C12 cells on SE50 showed 20% less attachment than SE100 after 1hr. hMSCs on SE 50 showed 8% higher cell attachment compared to on SE90 and SE100. (Scale bars: 200 μm)

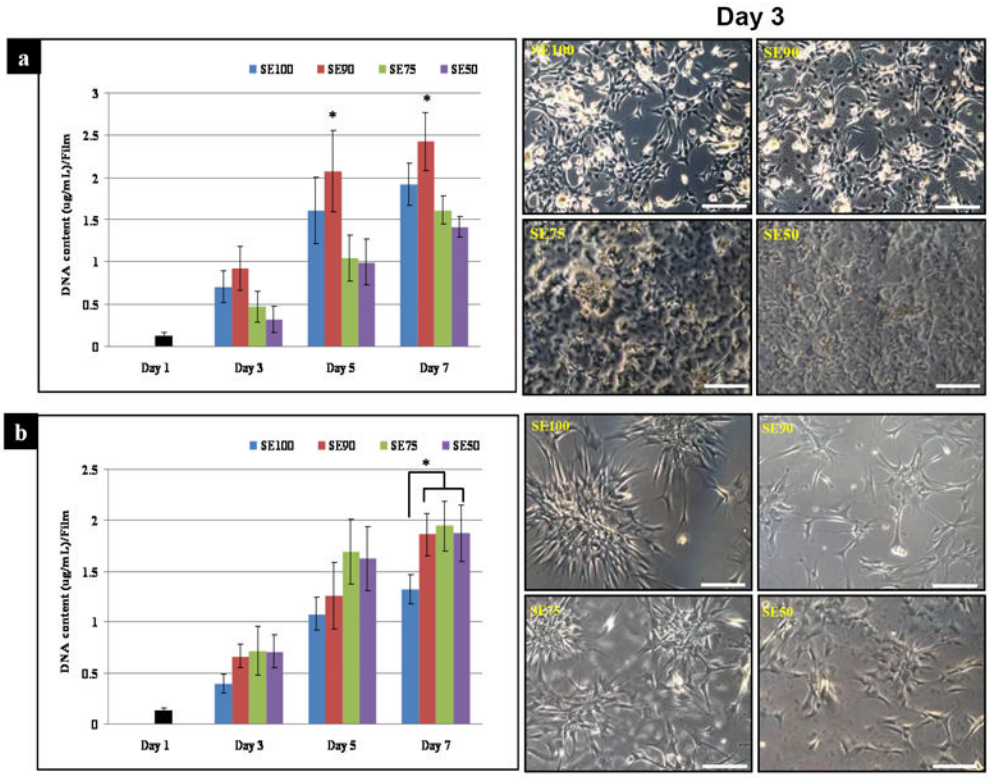

Figure 5.

Cell proliferation. (a) C2C12, (b) hMSCs. Cell proliferation of C2C12 cells on SE90 at day 7 was the highest among all groups, while hMSC proliferation on tropoelastin blends showed significantly higher levels than on SE100 at the same time points (*$p<0.05$). (Scale bars: 200 μm)

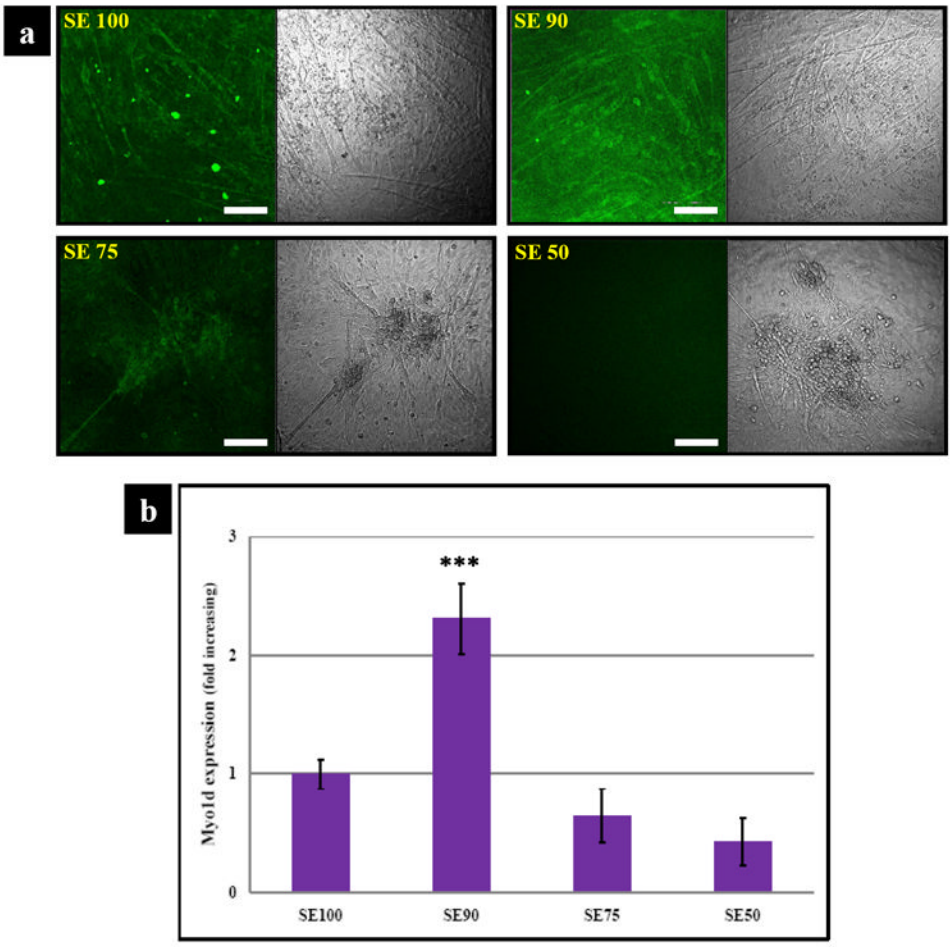

Figure 6.

Marker expression of myogenic induced C2C12 cells. (a) The molecular expression of Myo1d using immunocytochemical staining (scale bars: 150 μm); (b) Transcript levels of Myo1d. SE90 showed the highest Myo1d after 2 wk culture. SE90 exhibited 3 times higher myogenic transcript levels than SE75 and SE50 (***$p<0.001$).

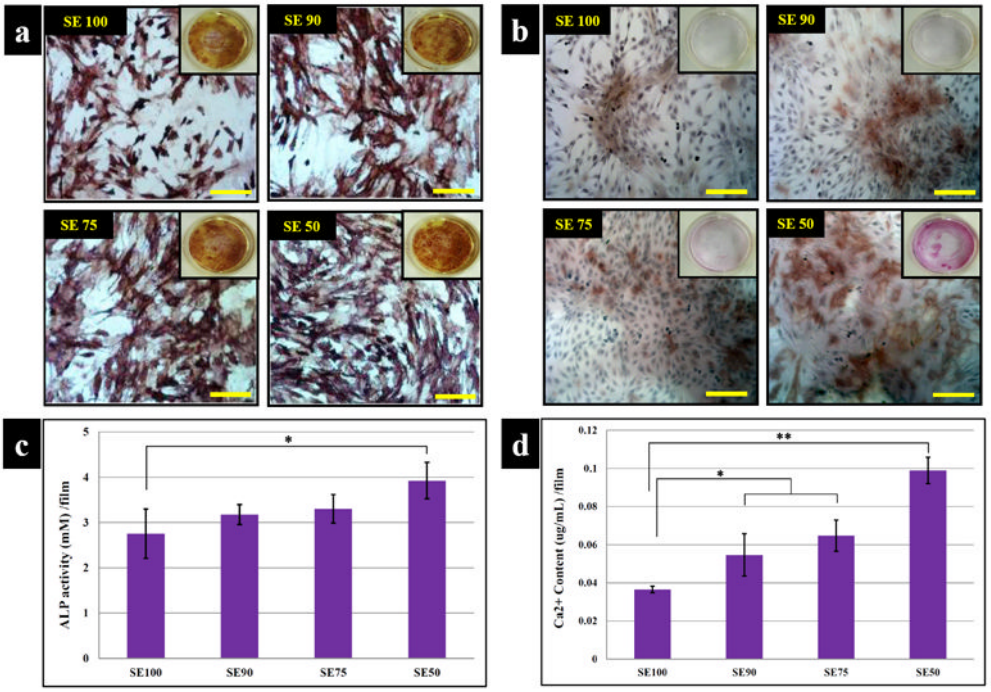

Figure 7.

Histological and chemical characterization of osteogenesis. (a) ALP and (b) Alizarin red. ALP activity as a marker of early osteoblastic differentiation displayed activity in all films at day 14 and levels on SE50 was significantly 1 increased when compared to the others samples. (Scale bars: 200 μm) (c) ALP activity per film, (d) calcium content per film with hMSCs cultured on the films in osteogenic medium. Staining of mineralized matrix after 2 wk in SE50 exhibited deeper color than on SE100. Increased calcium deposition was observed with increased tropoelasin content in the silk films. Data are mean ± standard deviation, from 4 samples, statistical differences (*$p<0.05$ and **$p<0.01$)

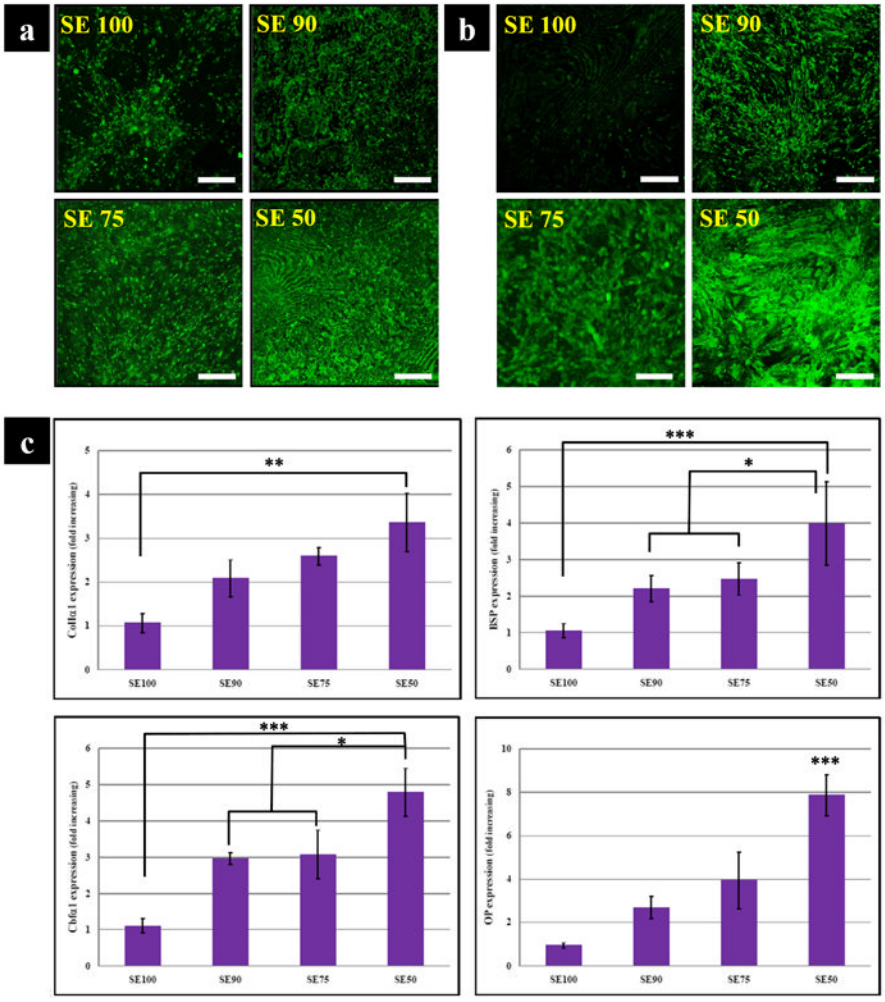

Figure 8.

Marker expressions of osteogenic induced hMSC. Immunocytochemical staining of osteogenic related ECM (a) BSP (b) OP. SE50 exhibited stronger staining at 2 wk than SE100 for both BSP and OP. (Scale bars: 150 μm) (c) Profile of osteogenic transcript levels; colIα1, BSP, OP and Cbfα1. Col Iα1 transcript level on SE50 was upregulated at 2 wk when compared to SE100. At this time point, the mRNA levels of BSP and OP were higher overall on the tropoelastin blend silks than in SE100. (*$p<0.05$, **$p<0.01$, and ***$p<0.001$).